JOURNAL OF PROPULSION AND POWER
Vol. 14, No. 2, March–April 1998

Aerodynamic Shape Optimization of a Subsonic Inlet Using Three-Dimensional Euler Computation

D. R. Reddy*
NASA Lewis Research Center, Cleveland, Ohio 44135
E. S. Reddy†
NYMA, Inc., Brook Park, Ohio 44142
and
R. E. Moody‡
The Boeing Company, Seattle, Washington 98124

A design optimization study of a subsonic inlet is presented where the peak Mach number at cruise condition on the inside of the inlet surface is the objective function to be minimized and inlet lip shape parameters are the design variables. The peak Mach number at takeoff, rolling takeoff, static, and crosswind conditions are constrained to an upper limit. The three-dimensional flowfield is predicted by the NPARC computational fluid dynamics code in Euler mode. A GRAPE- (grids about airfoils using Poisson's equation) based three-dimensional grid generator is employed to generate a C-grid around the inlet. Constrained numerical optimization is carried out by interfacing NPARC with the automated design synthesis optimization code. The constrained optimum is obtained by the method of feasible directions. The required gradients for optimization are computed via forward difference scheme. At the baseline (initial) design, takeoff, rolling takeoff, and crosswind conditions have their peak Mach numbers exceeding the upper bounds. However, at the constrained optimum design, only the upper limit on the takeoff peak Mach number is found to be critical with no appreciable change in cruise Mach number.

Nomenclature

a, b	=	major and minor radii of the superellipse
M	=	Mach number
n, m	=	superellipse exponents
X, Y, Z	=	global coordinates
x, y, z	=	local coordinates
α	=	angle of attack
β	=	yaw angle
θ	=	polar coordinate

Subscripts

c	=	crown
cw	=	crosswind
k	=	keel
rtof	=	rolling takeoff
st	=	static
tof	=	takeoff
∞	=	freestream

Introduction

WITH the advent of high-speed computers and the availability of more accurate and reliable computational fluid dynamics (CFD) solvers, numerical optimization processes can be effectively used to carry out aerodynamic shape design for optimum performance.[1–5] Compared to traditional methods such as wind-tunnel testing, this process involves modest cost and can be completed in a short period of time. However, the computational cost involved and time required are still functions of the flow model and grid size. The Navier–Stokes equations require more computational time to solve than the Euler equations, but they provide a more accurate representation of the flowfield. Similarly, a fine grid will require more computational time than a coarse grid, but it will also produce a more accurate result. Because of the iterative nature of the optimization process and large number of function evaluations involved, it is desirable to keep the computational cost of the CFD analysis low without compromising the accuracy too much. In an earlier study,[6] to improve the design of the engine inlet for a commercial transport aircraft, a potential solver was used instead of the expensive and time-consuming Navier–Stokes solvers. The design process was further simplified by employing a method called statistical design of experiments,[7] with a limited number of analyses for five operating conditions, namely, cruise, takeoff, rolling takeoff, static, and crosswind. But the study concluded that the results were not satisfactory.[6]

In the present work, efforts are made to define and carry out aerodynamic shape optimization of the inlet described in Ref. 6 using three-dimensional Euler computation and numerical optimization technique. Optimizing an inlet performance requires balanced tuning of various parameters across a wide range of flow conditions encountered during the operation of an aircraft. The shape of the inlet lip needs to be contoured to provide a gradual turning to minimize internal flow separation while maintaining moderate diffuser area ratios. The contouring is designed to eliminate high adverse pressure gradients that lead to flow separation or thickening of boundary layers that result in increased total pressure losses. Based on the experience of the inlet designers,[6] the peak Mach number inside the inlet is selected as a single parameter that represents the overall quality of the flowfield in the inviscid limit in relation to the inlet performance. The minimization of the peak Mach

Received May 5, 1997; revision received Sept. 16, 1997; accepted for publication Sept. 26, 1997.

*Senior Scientist, Propulsion Systems, 21000 Brookpark Road, M/S 5-11.
†Senior Research Engineer, Aeromechanics, 2001 Aerospace Parkway.
‡Senior Specialist Engineer, Propulsion Technology and Product Development, P.O. Box 3707, M/S 49-53.

number inside the inlet is observed to correlate to the maximum pressure recovery at the engine fan by reducing the shock losses and diffusion rates. Thus, the choice of the peak Mach number as an objective function makes it possible to use potential or Euler codes in place of Navier–Stokes codes. The potential code used by Mason et al.[6] does not allow geometry perturbations to be automated, which is an essential feature for numerical shape optimization. Hence, the NPARC code,[8] which has been in extensive use for the last 15 years by aerospace companies and government agencies, is selected for CFD calculations in the Euler mode. The objective is to seek an inlet shape that is optimum for all operating conditions.

Preliminary results of an initial study were reported in Ref. 9, where only three operating conditions, namely, cruise, takeoff, and rolling takeoff were considered. The sum of peak Mach numbers at takeoff and rolling takeoff and the square of their deviation was minimized in that study while constraining the cruise value to that at the initial design. In view of the fact that the engine will be running at a cruise condition the majority of the time compared to other conditions, the design optimization problem is revised in the current study to minimize the peak Mach number at a cruise condition while constraining the peak Mach numbers at takeoff, rolling takeoff, static, and crosswind conditions. The geometry and bounds of the variables used are the same as those used in Ref. 6. Freestream and compressor face conditions, angle of attack, and yaw angles for various operating conditions are given in Table 1.

The inlet considered is geometrically symmetric about a 0–180-deg plane (Fig. 1). For the cases of cruise and static conditions (zero yaw) the flowfield is also symmetric about a 0–180-deg plane and, hence, only one-half of the inlet is modeled. However, as a result of nonzero yaw, the entire inlet (0–360 deg) is modeled for takeoff, rolling takeoff, and crosswind conditions. Within each optimization cycle a fixed number of iterations are used for each run of the NPARC code. The interface of NPARC with the numerical optimization code, called automated design synthesis (ADS) (Ref. 10) is set up on a Cray C-90 as a shell script. The required gradients for optimization are computed via a forward difference scheme.

The optimum inlet shape that minimizes the cruise peak Mach number while satisfying the remaining operating conditions is formulated as a constrained optimization problem. The method of feasible directions[11] is used to obtain the constrained optimum. Numerical results are discussed along with the flowfield at the initial and optimum designs.

Table 1 Numerical data for various operating conditions

Operating condition	M_∞	α, deg	β, deg	M_c
Cruise	0.84	4.0	0	0.600
Takeoff	0.274	26.4	8.826	0.603
Rolling takeoff	0.106	0	26.5	0.589
Static	0.01	0	0	0.586
Crosswind	0.023	0	90.0	0.586

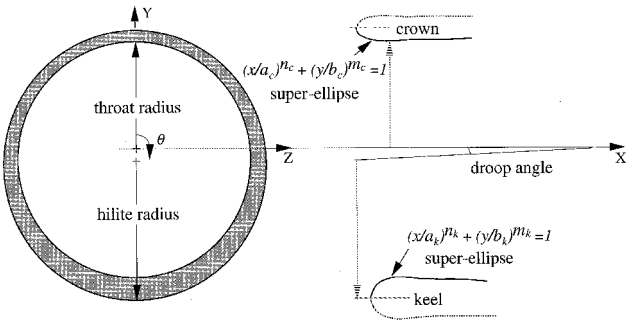

Fig. 1 Inlet cross section and lip geometry.

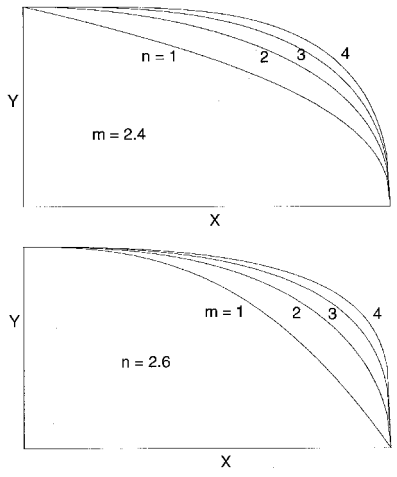

Fig. 2 Variation of superellipse shape with n and m.

Inlet Geometry

The inlet contour governs the delivery of air to the engine fan and thus plays a significant role in engine performance. Aspects of the inlet contour such as lip shape, contraction ratio, and drooping can be optimized to achieve the desired flow conditions at the fan. The basic inlet geometry used in this work is the same as the one reported in Ref. 6, and a schematic of the inlet is shown in Fig. 1. The inlet lip shape, i.e., the contour from the hilite to the throat, is described by a superelliptical curve that provides a high degree of flexibility through the variation of four parameters. The form of the superellipse used here is given by

$$(x/a)^n + (y/b)^m = 1 \tag{1}$$

where x is measured in the axial direction, y is measured in the radial direction, and a and b are the lengths of the major and minor axes, respectively (Fig. 2).

Because the inlet lip shape must perform well at multiple operating conditions with varying angles of attack and yaw angles, design optimization requires that the lip shape vary in the θ or angular direction from crown to keel. To minimize the installation drag, an inlet is drooped or oriented so that the hilite plane is perpendicular to the oncoming flow. Thus, efficient turning of airflow must be accomplished by the inlet between the hilite plane and the inlet attachment flange.

CFD Analysis

Computational Grid

The design optimization process involves changes in the lip shape and, hence, in the computational grid. The natural choice for the type of grid that adapts to changes in the shape would be a C-grid. For a single analysis, the conventional method of a generating grid is to use one of the commercially available interactive grid generation packages starting from the geometry definition obtained either manually or through a computer-aided design (CAD) interface. However, it is very time consuming and impractical to stop the design iterations and interactively generate the grid every time. To alleviate this problem, a three-dimensional grid generator based on the GRAPE (grids about airfoils using Poisson's equation) code,[12] that can be run in a batch mode, is selected and adapted for this study. In each θ plane inlet lip shape parameters and boundary grid points are defined and the GRAPE code is used to generate a smooth grid in the entire plane. A flowchart of the grid generation process is shown in Fig. 3.

For the inlet under consideration, the geometry is symmetric about a 0–180-deg plane and, hence, the grid is generated for only one-half of the inlet. The grid for the other half is generated

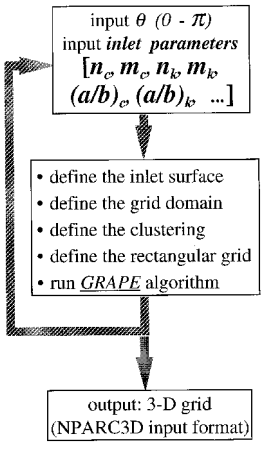

Fig. 3 Flowchart to generate C-grid for a three-dimensional inlet.

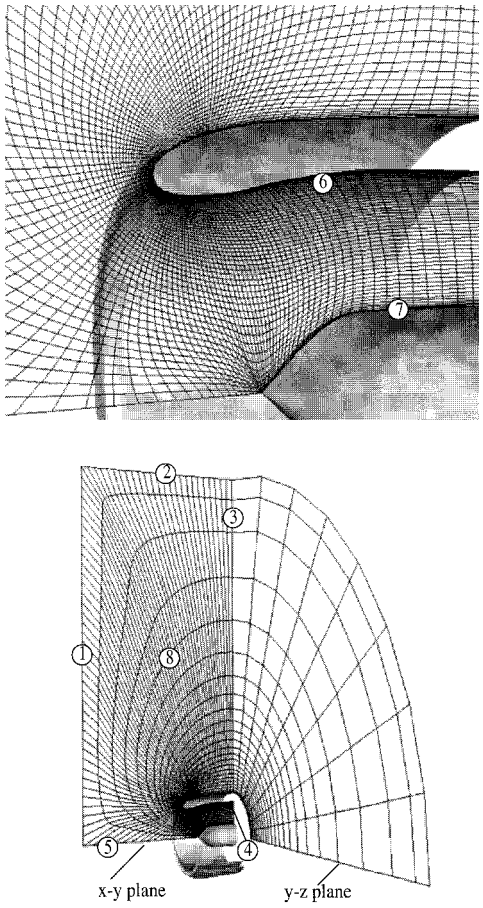

Fig. 4 C-grid for Euler computation: a) close view of the grid inside the inlet and b) sample three-dimensional grid in two planes (alternate grid lines shown in radial direction).

by reflection. Because the flow is symmetric about the vertical plane for zero yaw, only one-half of the inlet with a grid size of 130 × 55 × 17 (130 along C curve, 55 from nacelle to outer boundary, and 17 along the θ direction) is used for the computation. For the nonzero yaw case, the grid size is 133 × 55 × 33, spanning the full inlet. The distribution and the density of the grid used for the study are shown in Fig. 4. The size of the numerical grid for the computation used in this study is based on the mesh resolution required for the Euler computation to produce a grid-independent solution and is determined from a number of computations on grids of varying resolution.

Numerical Method

As mentioned previously, the NPARC code in the Euler mode is used to predict the flowfield. The code was originally developed as AIR3D by Pulliam and Steger,[13] and Pulliam[14] later added the artificial dissipation of Jameson et al.[15] and called the code ARC3D. Cooper et al.[16] adapted the code for internal flows of propulsion application and named the code PARC3D, which was subsequently renamed NPARC (Ref. 8) when an alliance was formed between NASA Lewis Research Center and the Arnold Engineering and Development Center to jointly develop and support the code. The alliance is currently very active in enhancing and supporting the code for a wide range of aerospace applications.

NPARC solves the full three-dimensional Reynolds-averaged Navier–Stokes equations in strong conservation form using Beam and Warming approximate factorization. The discretization employs central differencing on a generalized curvilinear coordinate system with implicit and explicit second- and fourth-order artificial dissipation. The fourth-order dissipation is added as a background damping to prevent odd and even point decoupling. The second-order dissipation is added primarily to smooth out oscillations in regions of pressure gradients associated with shock waves. There are several options available in the NPARC code to modify the amount of artificial dissipation added as described earlier. The option used in the present computations provides for an appropriate anisotropic model for the dissipation coefficients as suggested by Siclari et al.[17] Thus, the amount of the artificial dissipation added becomes more a function of the coordinate direction that depends on the local velocity component in each direction. A detailed description of all the available options of artificial dissipation treatment can be found in the report of Cooper and Sirbaugh.[18] To simplify the solution of the block pentadiagonal system of discretized equations, the block implicit operators are diagonalized by decomposing the flux Jacobians, resulting in a scalar pentadiagonal system. The loss of time accuracy from the diagonalization does not affect the spatial accuracy of the steady-state solution.[14]

The code has been verified by several investigators for a variety of flow configurations, demonstrating the accuracy of the flow during the course of its evolution to the present state. In the following text, some of the studies that are relevant to the flow configuration considered here are discussed. Although a majority of the studies involved viscous computations, the inviscid features that dominate the flowfield are similar to those in the present flow configuration. Hence, the numerical accuracy of the code established through these studies is considered to be the same for the present study. This is the primary reason for selecting the NPARC code for analysis, so that the focus of the investigation is on optimization rather than the accuracy of the analysis method.

DeBonis[19] applied NPARC to study the mixing performance of a mixer/ejector nozzle for a future supersonic transport application. Iek et al.[20] studied the flowfield within an inlet for an advanced ducted propeller at various angles of attack using NPARC and compared the solution with experimental data. Harloff et al.[21] applied NPARC to compute the three-dimensional flowfield in an S-duct of circular-to-rectangular transitioned cross section and presented a detailed comparison of results with the experimental data. Georgiadis and Yoder[22] examined three types of nozzle configurations with flow characteristics similar to those considered for a supersonic transport program to assess two different turbulence models. Lam[23] used NPARC in the Euler mode to estimate the off-design transonic performance of an over/under turbojet nozzle. DeBonis et al.[24] validated NPARC for two-dimensional and axisymmetric nozzle afterbody flows at transonic speeds using two-equation and zero-equation turbulence models to predict separation in the flowfield. Reddy[25] used NPARC to study the three-dimensional flowfield of a crossing, glancing shocks/turbulent boundary-layer interaction configuration to assess the predictive capability of NPARC for high-speed aircraft inlet application. Khavaran and Georgiadis[26] applied NPARC using simplified noise source correlation terms derived from acoustic

analogy to predict the three-dimensional directivity of noise for a Mach 1.5 elliptic jet as well as a round jet. Khalid and Morky[27] applied NPARC in the inviscid mode to study the wall interference effect on a finite thickness airfoil in a wind-tunnel test section.

Boundary Conditions

The boundary conditions for the computational domain, shown in Fig. 4b, are typical of those for any density-based time-marching scheme and are selected from the existing options of the NPARC code. At the inflow boundary (labeled 1 in Fig. 4), total pressure and temperature are specified, and at the outflow boundary (4), static pressure computed from the specified Mach number at the fan face is imposed. Freestream conditions are specified at the far-field boundaries (2 and 3). Slip (tangency) conditions are imposed on the solid walls (6 and 7), and the averaging condition is specified along the singular boundary of the inlet centerline ahead of the centerbody (5). Complete details of various boundary conditions and their implementation in the code are given in Ref. 8. For the computation at the cruise condition, the symmetry condition is applied at $\theta = 0$ and 180 planes (8 and 9, 9 is the $X-Z$ plane and is not shown in Fig. 4) because the flowfield is symmetric about the yaw axis.

Design Optimization

Optimization Interface

To carry out the numerical optimization process, the ADS code is interfaced with the NPARC CFD code and the grid generation code. Because the NPARC is a stand-alone code, the restart capability of ADS is utilized in the interface. A typical interface of an optimizer with CFD and grid generator codes is shown in Fig. 5.

The constrained problem is solved using the method of feasible directions. To minimize the turnaround time on a Cray C-90, a batch job is set up with one function evaluation. One function evaluation includes executing ADS, grid generation, and NPARC runs for all of the operating conditions. The CPU time required for one such job is approximately 6800 s.

Design Variables

The operating conditions considered have angles of attack and/or yaw and, hence, the inlet lip shapes at crown and keel are treated as independent. The six design variables used in the optimization study are the two exponents at the crown (n_c and m_c), two exponents at the keel (n_k and m_k), and ellipse radii ratios at crown keel (a_c/b_c and a_k/b_k). The bounds of these variables are given in Table 2. The ellipse exponents and a/b ratios at any intermediate angles are linearly interpolated. The outside profile is fixed and other parameters such as droop angle, droop length, and contraction ratios are not included as design variables in the present work.

Table 2 Design variables and bounds

Variable	Lower bound	Upper bound
n_c	2.0	2.6
m_c	1.6	2.4
n_k	2.0	2.6
m_k	1.6	2.4
a_c/b_c	2.5	3.0
a_k/b_k	2.0	2.5

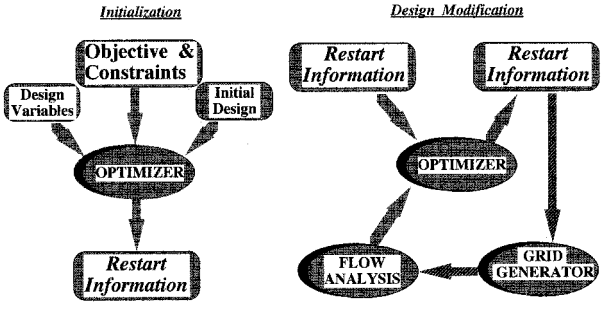

Fig. 5 Typical optimization interface with a CFD code.

Objective Function and Constraints

In Ref. 6, an optimum inlet design work was attempted that maximizes inlet performance during cruise and satisfies a set of constraints at the remaining operating conditions. These conditions were determined from the authors' previous inlet design experience, and are as follows: 1) peak Mach number at takeoff condition < 1.55, 2) peak Mach number at rolling takeoff condition < 1.45, 3) peak Mach number at static condition < 1.60, and 4) peak Mach number at crosswind condition < 1.60. In this study, the previous problem is formulated as a constrained numerical optimization problem. The optimization problem can be stated as follows:

find {inlet shape parameters} to minimize {max(M_{cr})}
subject to the following constraints.
max (M_{tof}) < 1.55
max (M_{rtof}) < 1.45
max (M_{st}) < 1.60
max (M_{cw}) < 1.60

Results and Discussion

For the initial geometry, convergence of the flow solution is studied for the cruise condition, and the mass flux residual is shown as a function of a number of iterations in Fig. 6. The residual decreases by more than two orders of magnitude and there is no appreciable change in the flowfield after 1000 iterations. Hence, for the entire optimization cycle, the number of iterations in each analysis (NPARC run) are fixed at 1000. During the optimization cycle, because the NPARC solution is used only to determine the sensitivity derivatives, the level of convergence achieved after 1000 iterations is found to be more than adequate. However, in the final analysis run, the residuals of all the governing equations are reduced by four orders of magnitude to achieve finer convergence. It is worth noting here that the flowfield (location and value of the peak Mach number) essentially remains the same after the residuals are reduced by two orders of magnitude.

Figure 7 shows the variation of the Mach numbers on the inside of the inlet surface of the initial geometry at the five operating conditions. At all operating conditions except the cruise, there is a strong shock on the inside of the lip. The peak Mach numbers for takeoff, rolling takeoff, static, and

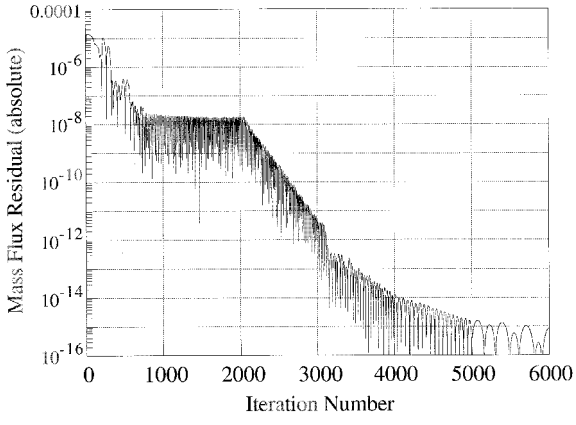

Fig. 6 NPARC convergence history for cruise condition at initial design.

crosswind conditions are 1.72, 1.58, 1.46, and 1.66, respectively. These distributions have similar magnitudes and patterns compared with those reported by Mason et al.[6] Note that the design parameters (superellipse parameters) used for the plots in Ref. 6 are not same as the initial design in the present work. In that study, the variables at the initial design were set at the bounds of their ranges; whereas in the present study, they correspond to the current design. Also, the angular positions at which the peaks occur were reported to be at 180, 180, 315, 0, and 180 deg for cruise, takeoff, rolling takeoff, static, and crosswind conditions, respectively. However, the corresponding values in this study are found to be 168.75, 202.5, 281.25, 22.5, and 281.25 deg. Because the flow is symmetric about the 0–180-deg plane for cruise and static conditions, one can expect the peak Mach number to occur at 180 and 0 deg. The discrepancy in the present results is found to be because of the way the symmetry condition is imposed numerically along the θ direction, which has a grid interval of 11.25 deg. Other factors that affect the location of the peak Mach number for other operating conditions are slight differences in the lip design variables and Euler flow analysis instead of the potential flow used in Ref. 6.

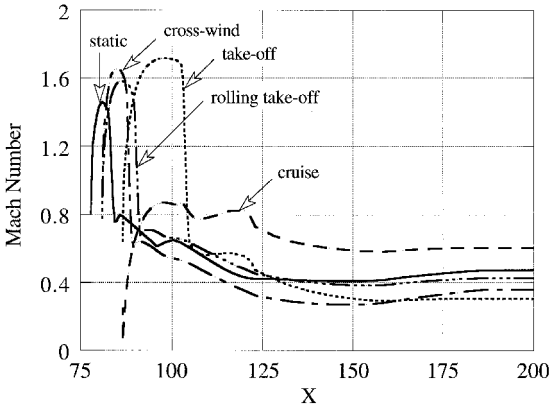

Fig. 7 Mach number variation along X at initial design.

Mach number contours are shown for each of the five operating conditions in Figs. 8–12 at the initial and optimum designs. The contours are shown for the angular plane that contains a maximum Mach number. As mentioned earlier, for the cruise condition, the flowfield does not show any significant difference between initial and optimum design (Figs. 8a and 8b). For the takeoff condition on the other hand (Figs. 9a and 9b), the shock strength for the optimum design is considerably less than that of the initial design. The plots for the remaining three operating conditions (Figs. 10–12) also show a significant reduction in the size of the supersonic flow region around the cowl when the design is optimized.

In the present computations, because Euler equations are solved, uniform static pressure computed from the average compressor-face Mach number is imposed at the exit plane of the inlet (outflow boundary). Comparison of the Mach number contours (not shown) for the initial and optimum designs show that the average Mach number is approximately the same for both designs, even though the flowfield appears to vary marginally.

The design parameters and the peak Mach numbers at initial and optimum design are given in Table 3. The optimum design is reached in seven iterations (Fig. 13) and all of the performance constraints are satisfied at the optimum. At the initial design, the peak Mach number for takeoff, rolling takeoff, and crosswind conditions exceeded the allowable limits, thereby violating the design constraints (Fig. 14). However, the design point is driven inside the feasible domain in the first iteration, while increasing the objective function (cruise peak Mach number). In subsequent iterations (two–seven) design modi-

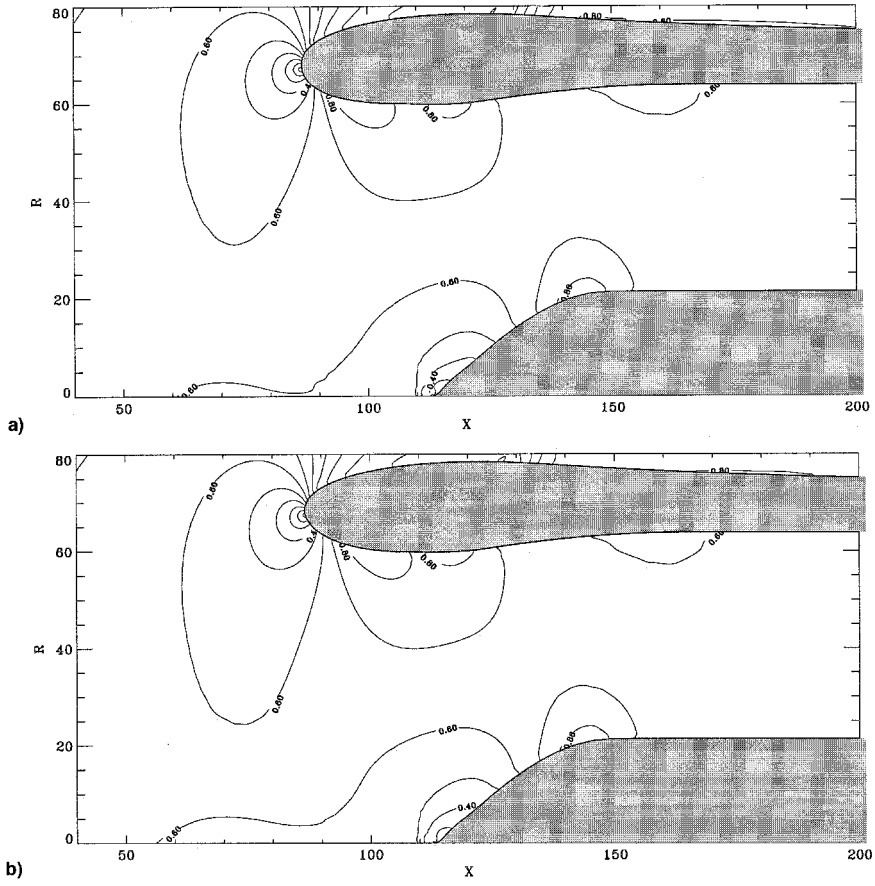

Fig. 8 Mach number contours at cruise condition: a) initial and b) optimum designs.

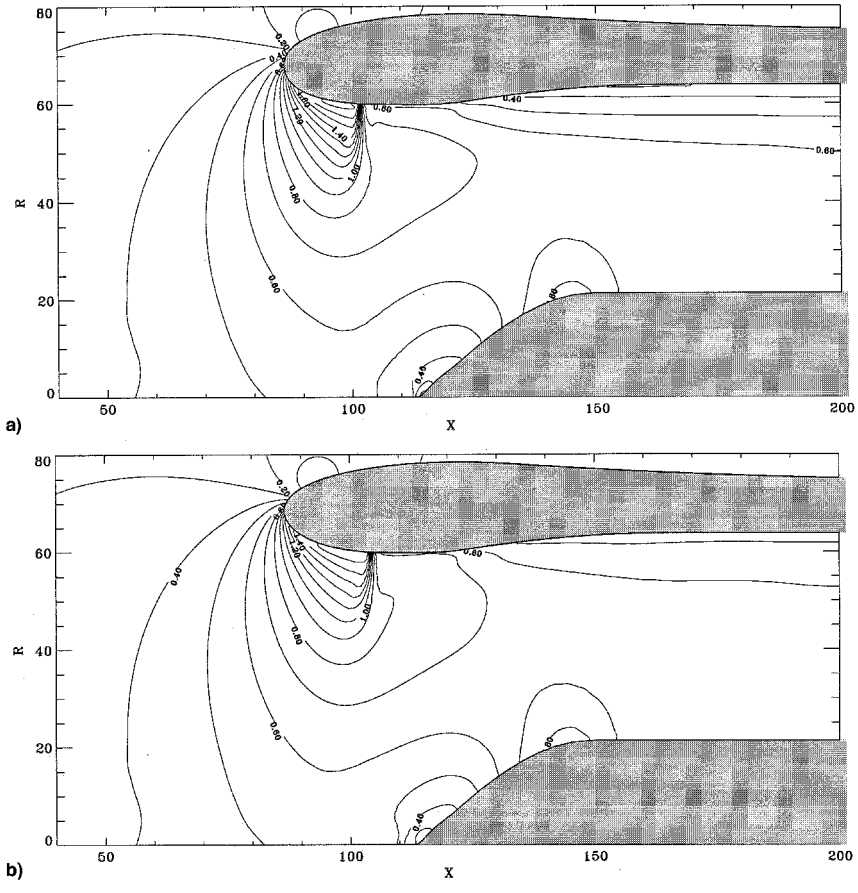

Fig. 9 Mach number contours at takeoff condition: a) initial and b) optimum designs.

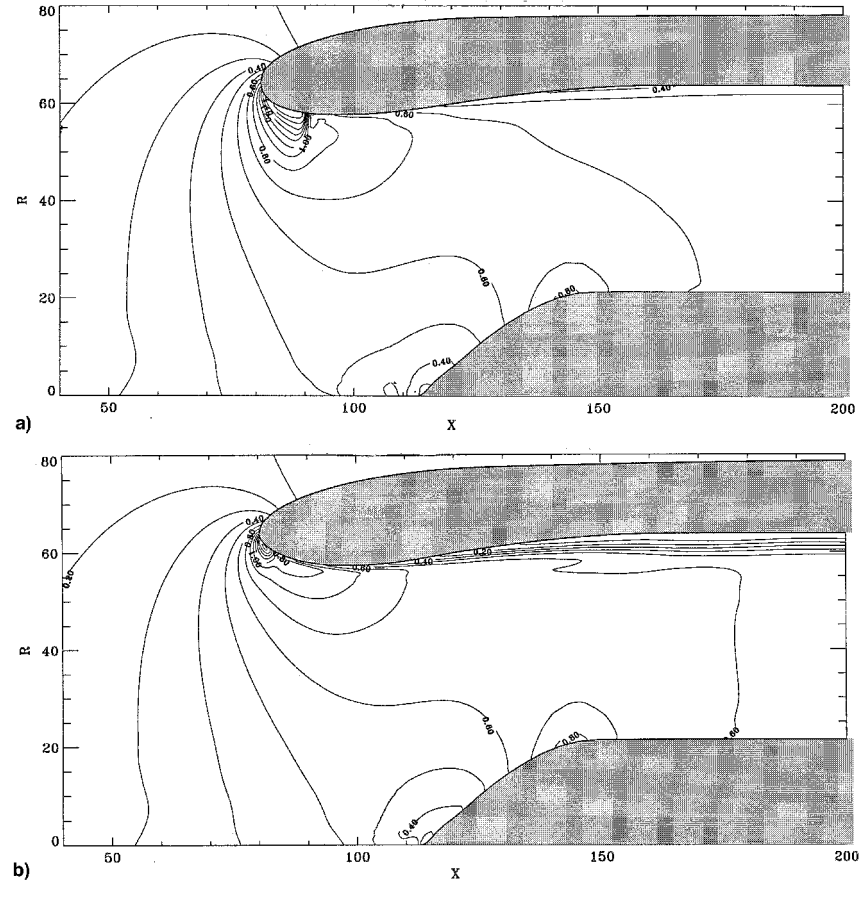

Fig. 10 Mach number contours at rolling takeoff condition: a) initial and b) optimum designs.

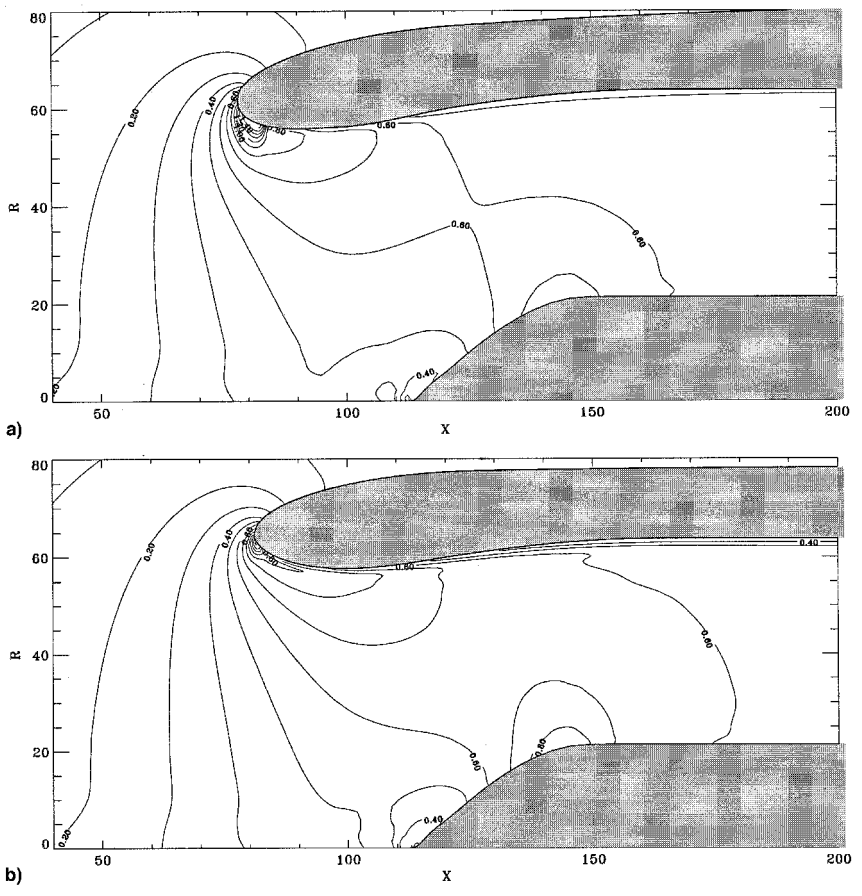

Fig. 11 Mach number contours at static condition: a) initial and b) optimum designs.

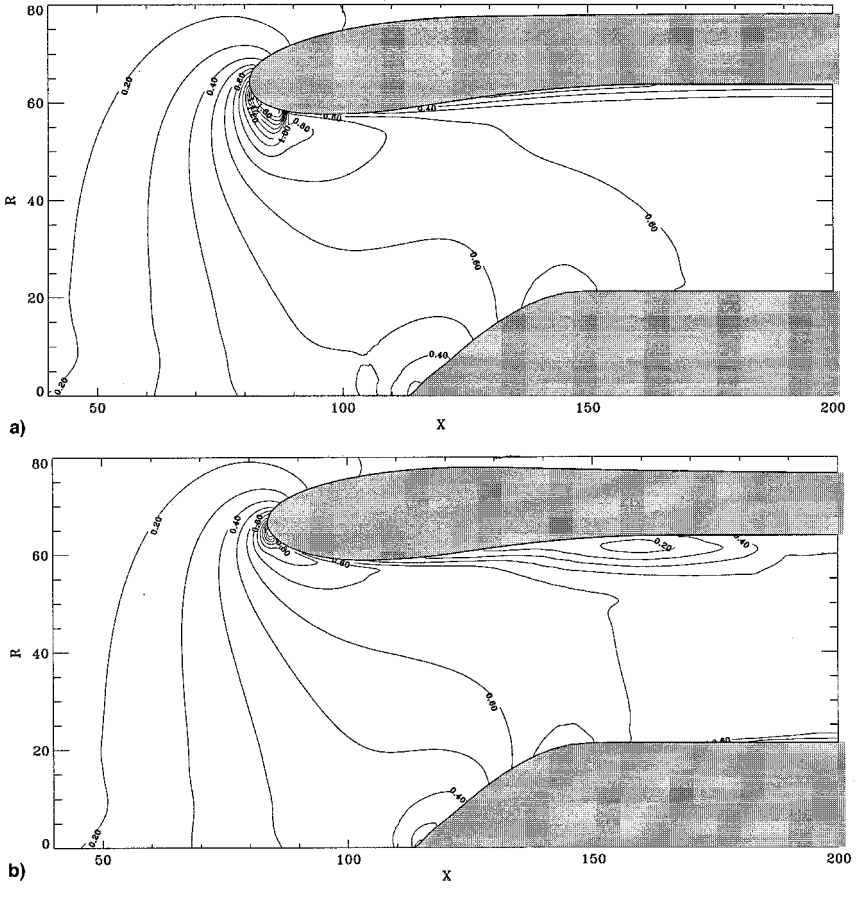

Fig. 12 Mach number contours at crosswind condition: a) initial and b) optimum designs.

Table 3 Summary of optimization results

Variable	Initial design	Optimum design
n_c	2.6	2.0
m_c	2.4	1.6
n_k	2.6	2.6
m_k	2.4	1.939
a_c/b_c	2.75	3.0
a_k/b_k	2.25	2.5
M_{cr}	0.8799	0.8918
M_{tof}	1.7156	1.5528
M_{rtof}	1.5825	1.3930
M_{st}	1.4595	1.3190
M_{cw}	1.6550	1.3881

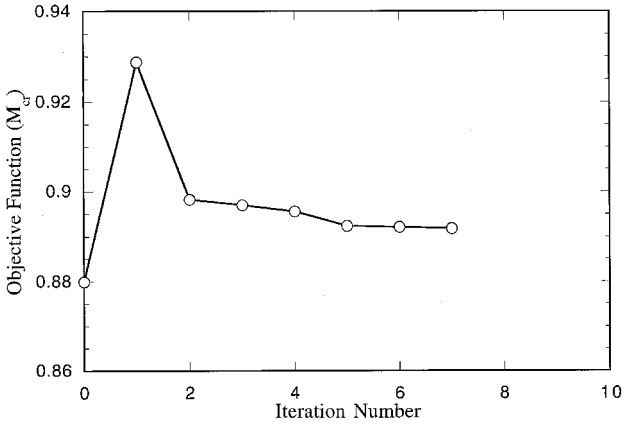

Fig. 13 Iteration history of the objective function.

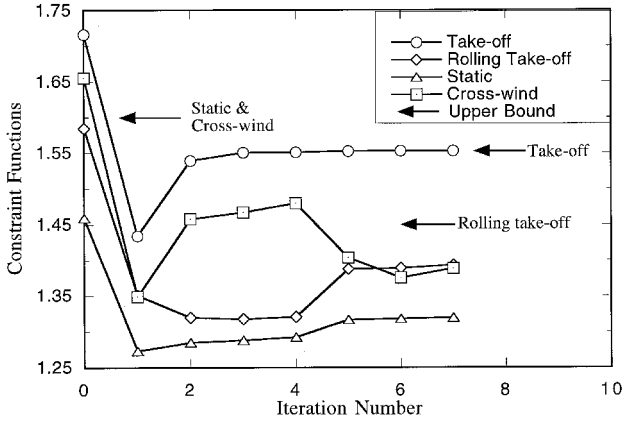

Fig. 14 Iteration history of the constraint functions.

fications resulted in bringing the objective function value near the starting value without any violation of performance constraints. At the optimum, only takeoff constraint ($M_{tof} < 1.55$) becomes critical, i.e., controls the design.

Figure 15 shows the inlet lip shapes at crown and keel. It can be seen that the optimum lip at the crown is longer, sharper, and steeper compared with the one at the initial design. This is because the exponents associated with the lip (n_c and m_c) are driven to lower bounds (2.0 and 1.6), and the a/b ratio is driven to the upper bound (3.0), i.e., major radius is greater than minor radius. On the contrary, the x exponent for the keel (n_k) reached upper bound (2.6), giving a less steep but longer lip profile. The keel's y exponent is either at the lower or upper limit as the design is controlled by the limit on the peak Mach number at takeoff condition and the peak occurs at or near the keel ($\theta = 180$).

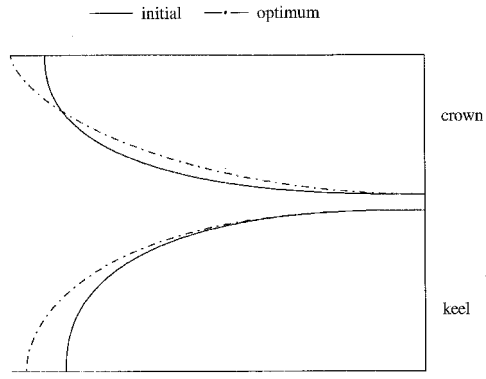

Fig. 15 Comparison of lip shapes at initial and optimum designs.

As presented in Figs. 8b–12b, the flowfield at the optimum design shows much weaker shocks for all of the operating conditions. The weaker shocks result in reduction of the shock losses as well as viscous losses caused by less severe shock/boundary-layer interaction. Even though the study has not considered the viscous losses, the reduction of the supersonic flow region and weaker shocks result in a considerable improvement in the total pressure recovery by minimizing the losses. If viscous flow analysis were to become affordable for these types of configurations, performance parameters such as total pressure recovery can be optimized directly with constraints on stability parameters or some other design criteria.

Summary

A numerical optimization procedure has been successfully developed to find the inlet shape that minimizes the peak Mach number at cruise while satisfying the peak Mach number constraints at other operating conditions, namely, takeoff, rolling takeoff, static, and crosswind. Also, the three-dimensional Euler code is found to be a useful tool to carry out the inlet optimization. For the subsonic inlet geometry considered in this paper, off-design requirements have been satisfied without adversely affecting the cruise performance. The upper bound on the peak Mach number at takeoff is found to be controlling the optimum design. The crown superellipse has a sharp and steep lip, whereas the keel superellipse has a long and less steep lip at the final design. Results could be further improved by including droop angle, droop length, and contraction ratio as design variables. A more flexible lip variation along the circumference can also be included as a parameter in the study, i.e., the lip parameters at more θ locations can be included as design variables.

Acknowledgments

E. S. Reddy was supported by NASA Lewis Research Center under Contract NAS3-25266. The authors would like to thank Gary Harloff of NYMA for useful discussions during the course of this investigation.

References

[1]Baysal, O., and Eleshaky, M. E., "Aerodynamic Design Optimization Using Sensitivity Analysis and Computational Fluid Dynamics," AIAA Paper 91-0471, Jan. 1991.

[2]Stookesbury, D., Verhoff, A., and Cain, A. B., "An Efficient Approach to Optimal Aerodynamic Design Part 2: Implementation and Evaluation," AIAA Paper 93-0100, Jan. 1993.

[3]Eyi, S., Hager, J. O., and Lee, K. D., "Airfoil Design Using the Navier-Stokes Equations," AIAA Paper 93-0648, Jan. 1993.

[4]Eyi, S., and Lee, K. D., "Inverse Airfoil Design Using the Navier-Stokes Equations," AIAA Paper 93-0972, Feb. 1993.

[5]Hager, J. O., Eyi, S., and Lee, K. D., "Design Efficiency Evaluation for Transonic Airfoil Optimization: A Case for Navier-Stokes Design," AIAA Paper 93-3112, July 1993.

[6]Mason, J. G., Farquhar, B. W., Booker, A. J., and Moody, R. E.,

''Inlet Design Using a Blend of Experimental and Computational Techniques,'' *Proceedings of the 18th ICAS Congress* (Beijing, China), Vol. 1, 1992, pp. 445–454.

[7]Box, G. E. P., Hunter, W. G., and Hunter, J. S., *Statistics for Experimenters*, Wiley, New York, 1978.

[8]''A User's Guide to NPARC,'' Version 2.0, The NPARC Alliance Team, NASA Lewis Research Center and Arnold Engineering Development Center, Nov. 1994.

[9]Reddy, E. S., and Reddy, D. R., ''Aerodynamic Shape Optimization of a Subsonic Inlet Using 3-D Euler Computation,'' AIAA Paper 95-2757, July 1995.

[10]Vanderplaats, G. N., ''ADS-A Fortran Program for Automated Design Synthesis,'' NASA CR 177985, Sept. 1985.

[11]Vanderplaats, G. N., *Numerical Optimization Techniques for Engineering Design*, McGraw–Hill, New York, 1984.

[12]Sorenson, R. L., ''A Computer Program to Generate Two-Dimensional Grids About Airfoils and Other Shapes by Use of Poisson's Equation,'' NASA TM 81198, May 1980.

[13]Pulliam, T. H., and Steger, J. L., ''Implicit Finite-Difference Simulations of Three Dimensional Compressible Flow,'' *AIAA Journal*, Vol. 18, No. 2, 1980, pp. 159–167.

[14]Pulliam, T. H., ''Euler and Thin Layer Navier-Stokes Code: ARC2D, ARC3D,'' *Notes for Computational Fluid Dynamics User's Workshop*, Univ. of Tennessee Space Inst., Tullahoma, TN, March 1984.

[15]Jameson, A., Schmidt, W., and Turkel, E., ''Numerical Solutions of the Euler Equations by Finite Volume Method Using Runge-Kutta Time Stepping Schemes,'' AIAA Paper 81-1259, June 1981.

[16]Cooper, G. K., Jordan, J. L., and Phares, W. J., ''Analysis Tool for Application to Ground Testing of Highly Underexpanded Nozzles,'' AIAA Paper 87-2015, June 1987.

[17]Siclari, M. J., DelGuidice, P., and Jameson, A., ''A Multigrid Finite Volume Method for Solving the Euler and Navier-Stokes Equations for High Speed Flows,'' AIAA Paper 89-0283, 1989.

[18]Cooper, G. K., and Sirbaugh, J. R., ''PARC Code: Theory and Usage,'' Arnold Engineering Development Center, TR-89-15, Tullahoma, TN, Dec. 1989.

[19]DeBonis, J. R., ''Full Navier-Stokes Analysis of a Two-Dimensional Mixer/Ejector Nozzle for Noise Suppression,'' AIAA Paper 92-3570, July 1992.

[20]Iek, C., Boldman, D. R., and Ibrahim, M., ''Analysis of an Advanced Ducted Propeller Subsonic Inlet,'' AIAA Paper 92-0274, Jan. 1992.

[21]Harloff, G. J., Reichert, B. A., Sirbaugh, J. R., and Wellborn, S. R., ''Navier-Stokes Analysis and Experimental Data Comparison of Compressible Flow Within Ducts,'' NASA TM-105796, July 1992.

[22]Georgiadis, N. J., and Yoder, D. A., ''Use of Navier-Stokes Methods for the Calculation of High-Speed Nozzle Flow Fields,'' AIAA Paper 94-3212, June 1994.

[23]Lam, D. W., ''Use of the PARC Code to Estimate the Off-Design Transonic Performance of an Over/Under Turbojet Nozzle,'' AIAA Paper 95-2616, July 1995.

[24]DeBonis, J. R., and Georgiadis, N. J., ''Validation of the NPARC Code for Nozzle Afterbody Flows at Transonic Speeds,'' AIAA Paper 95-2614, July 1995.

[25]Reddy, D. R., ''3-D Navier-Stokes Analysis of Crossing Glancing Shocks/Turbulent Boundary Layer Interactions,'' *Computers and Fluids Journal*, Vol. 24, No. 4, 1995, pp. 435–445.

[26]Khavaran, A., and Georgiadis, N. J., ''Aeroacoustics of Supersonic Elliptic Jets,'' AIAA Paper 96-0641, Jan. 1996.

[27]Khalid, M., and Morky, M., ''An NPARC Study of a Two-Dimensional Wall Interference,'' AIAA Paper 96-0496, Jan. 1996.